JCTC Journal of Chemical Theory and Computation

Classical Calculation of Transient Absorption Spectra Monitoring Ultrafast Electron Transfer Processes

Igor Uspenskiy, Birgit Strodel, and Gerhard Stock*

Institute of Physical and Theoretical Chemistry, J. W. Goethe University, Max-von-Laue-Str. 7, D-60438 Frankfurt, Germany

Received June 28, 2006

Abstract: Classical formulations are considered that allow for the calculation of time- and frequency-resolved pump−probe spectra of nonadiabatically coupled molecular systems. When the semiclassical Franck−Condon approximation in the theoretical framework of the doorway-window formalism is employed, various first- and second-order expressions for the classical doorway and window functions are derived. Moreover, a classical analogue of the electronic dipole transition operator is employed. When established models describing ultrafast photoinduced electron transfer are adopted, it is found that the first-order approximations give rise to spurious structures of the time-resolved signal, which indicate that these approximations fail to correctly account for the averaging effect caused by finite pulses. The higher-order approximations, on the other hand, are shown to give a fairly accurate description of the transient absorption spectrum. By comparing to exact quantum-mechanical calculations, the merits and shortcomings of the various approaches as well as the generally achievable accuracy of a classical modeling of optical spectra is discussed.

I. Introduction

Significant progress in femtosecond time-resolved spectroscopy has made it possible to observe elementary photochemical reactions in real time.[1] Because the interpretation of these experiments often represents a nontrivial problem, a theoretical modeling of photoinduced processes and their spectroscopy is needed. In principle, the theory of nonlinear spectroscopy is well-developed.[2] In the majority of theoretical studies, however, the description of the chemical dynamics is based on rather simple models, usually a few-level system or a set of harmonic oscillators, which—in the case of condensed-phase spectroscopy—may be coupled to a thermal bath. To facilitate the description of photophysical and photochemical reactions, several groups have constructed ab initio based multidimensional model Hamiltonians and performed time-dependent wave packet calculations.[3] The main bottleneck of this approach is the cumbersome and often impossible task of precomputing the relevant multidimensional potential energy surfaces of the system. To circumvent this problem, the theoretical description of photochemical reactions in terms of direct ab initio molecular-dynamics simulations has recently become popular.[4−6] Because the nuclear dynamics is treated classically in this approach, it is necessary to develop formulations that allow us to calculate nonlinear time- and frequency-resolved spectra from classical trajectories.[7−17]

In many cases, however, the theoretical description of photoinduced molecular dynamics is complicated by the fact that the underlying Born−Oppenheimer assumption of noninteracting adiabatic potential-energy surfaces may break down.[18−20] Nonadiabatic photoprocesses such as internal conversion, cis−trans photoisomerization, and electron transfer are prime examples. To account for this situation, multidimensional time-dependent wave packet calculations on coupled potential-energy surfaces as well as simulations of the corresponding femtosecond time- and frequency-resolved spectra have been reported.[3,8,20−22] To achieve a classical description of nonadiabatic quantum dynamics, various semiclassical theories as well as mixed quantum-classical schemes have been proposed,[23−26] most notably the "mean-field trajectory" approach and the "surface-hopping"

* Corresponding author fax: +49-69-798-29709; e-mail: stock@theochem.uni-frankfurt.de.

10.1021/ct6002127 CCC: $33.50
Published on Web 10/21/2006

approach. These methods share the concept that the electronic degrees of freedom are represented by a wave function description, while the nuclear degrees of freedom are represented by a trajectory description. Only a few papers,[27−29] though, have employed these methods to calculate optical spectra of nonadiabatically coupled systems.

In this work, we present several classical approximations to calculate time- and frequency-resolved pump−probe spectra. To this end, we generalize various versions of the so-called semiclassical Franck−Condon approximation[7,8,30] to the case of nonadiabatically coupled potential-energy surfaces. Alternatively, we employ the mapping approach[31] or classical electron analogue model[32] to define the classical analogon of the electronic dipole transition operator.[33] When these formulations are employed, explicit expressions for various cases of electron transfer are derived and compared. As representative examples, we adopt two established models describing ultrafast photoinduced electron transfer,[34,35] for which exact quantum-mechanical reference calculations are possible. Performing a detailed numerical study, the merits and shortcomings of the various approaches as well as the generally achievable accuracy of a classical modeling of optical spectra is discussed.

II. Quantum-Mechanical Formulation

A. Model. As a well-studied model of photoinduced electron transfer,[36] we consider an electronic three-state system, comprising an energetically well-separated electronic ground state $|\psi_0\rangle$ and two nonadiabatically coupled excited states $|\psi_1\rangle$ and $|\psi_2\rangle$ (see Figure 1a). It is assumed that the electron-transfer process takes place between the two excited electronic states after excitation of the system at time $t = 0$ by an ultrashort laser pulse from $|\psi_0\rangle$ to the optically bright state $|\psi_2\rangle$. When a diabatic electronic representation is adopted, the molecular Hamiltonian of an electron-transfer system can be written as[37]

$$H = \sum_{n,m} |\psi_n\rangle h_{nm} \langle\psi_m| = \sum_n |\psi_n\rangle h_n \langle\psi_n| + \{|\psi_1\rangle V_{12} \langle\psi_2| + \text{h.c.}\} \quad (2.1)$$

comprising the vibrational Hamiltonian $h_n = T + V_n$ in the diabatic electronic state $|\psi_n\rangle$ and the off-diagonal diabatic coupling elements V_{12}. To be specific, we adopt a spin-boson type of model,[38] that is, a constant diabatic coupling $V_{12} = V_{21} = g$ and harmonic diabatic potentials

$$V_n(x) = E_n + \sum_j \frac{1}{2}\omega_j x_j^2 + \kappa_j^{(n)} x_j \quad (2.2)$$

where E_n is the vertical excitation energy, ω_j denotes the frequency of the jth vibrational mode, and $\kappa_j^{(n)}$ represents the gradient of the excited-state potential-energy surface V_n along this mode. Throughout this paper, we set $\hbar \equiv 1$ and use dimensionless vibrational coordinates and momenta.

B. Electron-Transfer Dynamics. To study the dynamics of the electron-transfer model (eq 2.1), we solve the time-dependent Schrödinger equation to obtain the time-dependent wave function $|\Psi(t)\rangle$ as well as the density operator $\rho(t) = |\Psi(t)\rangle\langle\Psi(t)|$ of the system. As a suitable initial condition, we assume that at time $t = 0$ the system is impulsively prepared in the excited electronic $|\psi_2\rangle$. A key quantity in the discussion of photoinduced electron-transfer processes is the time-dependent population probability of the optically excited diabatic electronic state[20]

$$P_2(t) = \text{Tr}\{|\psi_2\rangle\langle\psi_2|\rho(t)\} \quad (2.3)$$

As $P_2(t)$ is constant in the absence of nonadiabatic coupling, the diabatic population directly monitors the electron-transfer process of interest. Furthermore, we consider the time-dependent probability distribution along a specific vibrational mode x

$$P_n(x,t) = \text{Tr}\{|\psi_n\rangle|x\rangle\langle x|\langle\psi_n|\rho(t)\} \quad (2.4)$$

in order to illustrate the vibrational motion of the laser-induced wave packet on the coupled potential-energy curves V_1 and V_2.

So far, the theory has been elaborated using *diabatic* electronic states $|\psi_n\rangle$. A diabatic electronic representation is advantageous for the interpretation of spectroscopic data, because in the vicinity of surface-crossings the electronic transition dipole operator is only smooth in the diabatic representation.[3] On the other hand, we may employ a unitary transformation that diagonalizes the diabatic potential matrix, which yields *adiabatic* electronic states $|\psi_n^{\text{ad}}\rangle$ and the

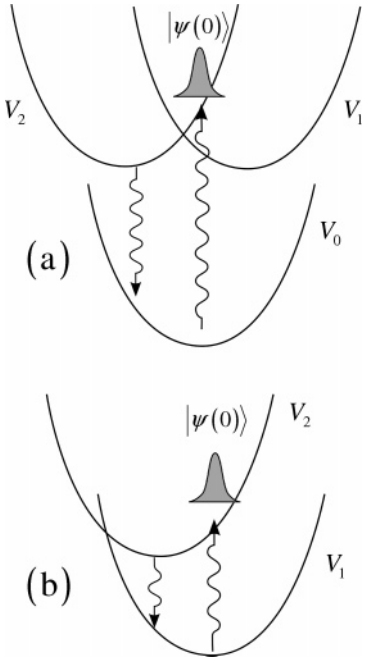

Figure 1. Schematic view of the diabatic potential-energy curves $V_n(x)$ pertaining to the two electron-transfer models under consideration. At time $t = 0$, the system is prepared by an impulsive pump pulse into a nonstationary state $|\Psi(0)\rangle$, whose time evolution is interrogated by a time-delayed probe pulse which may induce internal or external electronic transitions. (a) External case, i.e., the radiation field induces transitions from the two coupled excited-state potentials V_1 and V_2 to the electronic ground-state potential V_0. (b) Internal case, i.e., the radiation field induces transitions between the two coupled electronic states.

adiabatic potential-energy surfaces

$$W_{1/2} = \frac{1}{2}(V_1 + V_2) \mp \frac{1}{2}\sqrt{(V_2 - V_1)^2 + 4V_{12}} \quad (2.5)$$

For example, to discuss nonadiabatic relaxation processes such as electron transfer, it appears natural to consider the adiabatic population probability

$$P_2^{\mathrm{ad}}(t) = \mathrm{Tr}\{|\psi_2^{\mathrm{ad}}\rangle\langle\psi_2^{\mathrm{ad}}|\rho(t)\} \quad (2.6)$$

which monitors the decay of the "upper" adiabatic state $|\psi_2^{\mathrm{ad}}\rangle$ into the lower-lying electronic states.

C. Transient Absorption. In typical pump−probe experiments, the molecular system is prepared at time $t = 0$ by a first laser pulse (the "pump" ϵ_{I}) into a nonstationary state, whose time evolution is interrogated by a second laser pulse (the "probe" ϵ_{II}) at the delay time t_{d}. Let us furthermore assume that the excitation is resonant, thus resulting in a population of the excited state, and that the pump and probe pulses do not overlap, thus facilitating the interpretation of signals. Within the electric dipole approximation, the interaction between the molecular system and the external electric field is then given by

$$H_{\mathrm{int}}(t) = -\hat{\mu}[\epsilon_{\mathrm{I}}(t) + \epsilon_{\mathrm{II}}(t)]$$
$$\hat{\mu} = |\psi_0\rangle\mu_{02}\langle\psi_2| + |\psi_2\rangle\mu_{20}\langle\psi_0| \quad (2.7)$$
$$\epsilon_i(t) = 1/\sqrt{4\pi\alpha\tau_i^2}\, \mathrm{e}^{-(t-t_i)^2/(4\alpha\tau_i^2)}\, \mathrm{e}^{-i\omega_i(t-t_d)} + \mathrm{c.c.} \quad (2.8)$$

with $\alpha = 1/(16 \ln 2)$. The laser pulses are characterized by their carrier frequencies ω_{I} and ω_{II} and their durations τ_{I} and τ_{II}, respectively. They are centered at times $t = t_i$, where $t_{\mathrm{I}} = 0$ and $t_{\mathrm{II}} = t_{\mathrm{d}}$, representing the delay time of the probe pulse.

Adopting a doorway−window-type representation,[2,39] the quantum-mechanical pump−probe signal can be written as (see Appendix A)

$$I(t_{\mathrm{d}}) = \mathrm{Tr}\{\mathscr{W}\mathrm{e}^{-\mathrm{i}\mathscr{H}_d}\mathscr{D}\rho_0\} \quad (2.9)$$

where Tr denotes the trace over the electronic and vibrational degrees of freedom and ρ_0 represents the initial density operator of the molecular system prior to the interaction with the laser field. The Liouville operator $\mathscr{D}$ denotes the doorway operator describing the preparation of the system at time $t = 0$ by the pump pulse, $\mathscr{H}\cdots = [H,\cdots]$ is the molecular Liouvillian ($\hbar \equiv 1$), accounting for the time evolution of the molecular system during $0 \le t \le t_{\mathrm{d}}$, and $\mathscr{W}$ represents the window operator, describing the interaction of the system with the probe laser at $t = t_{\mathrm{d}}$.

Depending on the employed laser frequencies and the molecular system under consideration, several spectroscopic processes may contribute to the transient absorption signal (eq 2.9): the photoinduced excited-state population gives rise to stimulated emission and excited-state absorption, while the reduced population in the electronic ground state causes a bleach of the absorption band as well as impulsive stimulated Raman scattering.[2,40] In this work, we are particularly interested in the excited-state contribution to the transient absorption. In the limit of ultrashort probe pulses, the excited-state pump−probe signal measures the diabatic population probability $P_2(t)$ defined in eq 2.3[20] and therefore directly monitors the electron-transfer process of interest.

III. Classical Description of Nonadiabatic Dynamics

The classical description of the nonadiabatic dynamics has been the subject of numerous articles[23,24,26] and is only briefly reviewed here for further reference. The starting point of most mixed quantum-classical schemes such as the mean-field trajectory and the surface-hopping methods is to expand the total wave function in electronic states $|\psi_n\rangle$

$$|\Psi(t)\rangle = \sum_n d_n(\mathbf{x},t)|\psi_n\rangle \quad (3.1)$$

where $d_n(\mathbf{x},t)$ denotes the vibrational wave function pertaining to the electronic state $|\psi_n\rangle$. Employing Hamiltonian eq 2.1, we obtain for the time-dependent Schrödinger equation

$$i\dot{d}_n = \sum_m h_{nm}(\mathbf{x})\, d_m \quad (3.2)$$

To introduce the classical-path approximation, we assume that the nuclear dynamics of the system can be described by classical trajectories; that is, the position operator $\hat{\mathbf{x}}$ is approximated by its mean value, that is, the trajectory $\mathbf{x}(t)$. As a consequence, the quantum-mechanical *operators* of the nuclear dynamics [e.g., $h_{\mathrm{nm}}(\mathbf{x})$] become classical *functions* which depend parametrically on $\mathbf{x}(t)$. In the same way, the nuclear *wave functions* $d_n(\mathbf{x},t)$ become complex-valued *coefficients* $d_n[\mathbf{x}(t),t]$. As the electronic dynamics are evaluated along the classical path of the nuclei, the approximation thus accounts for the reaction of the quantum degrees of freedom to the dynamics of the classical degrees of freedom.

The back-reaction of the classical degrees of freedom to the dynamics of the quantum degrees of freedom may be described either self-consistently (in the mean-field trajectory method) or via a hopping algorithm (in the surface-hopping method). In the former, the classical force $F = \dot{p}_j$ acting on the nuclear degrees of freedom x_j is given as an average over the quantum degrees of freedom

$$\dot{p}_j = -\left\langle \Psi(t)\left|\frac{\partial H}{\partial x_j}\right|\Psi(t)\right\rangle \quad (3.3)$$

In the surface-hopping approach, on the other hand, the coupling of quantum and classical degrees of freedom is realized via instantaneous hops between coupled potential-energy surfaces, while the trajectories always propagate on a *single* adiabatic surface.[23]

Because in mixed quantum-classical methods electronic and nuclear degrees of freedom are treated on a different dynamical footing, these theories do not necessarily provide a satisfying classical picture of nonadiabatic dynamics. As an alternative approach to incorporate quantum degrees of freedom in a classical formulation, it has recently been proposed to utilize quantum-mechanical bosonization techniques, that is, to represent discrete electronic states by continuous harmonic oscillators, which possess a well-defined classical limit.[31,41] This is achieved by the mapping

relations

$$|\psi_n\rangle\langle\psi_m| \rightarrow \frac{1}{2}(X_n - iP_n)(X_m + iP_m) \tag{3.4}$$

$$|\psi_n\rangle \rightarrow |0_1, ..., 1_n, ..., 0_N\rangle \tag{3.5}$$

where X_n and P_n are position and momentum operators of the nth oscillator with commutation relations $[X_n,P_m] = i\delta_{nm}$, and $|0_1,..., 1_n,..., 0_N\rangle$ denotes a harmonic-oscillator eigenstate with a single quantum excitation in the mode n.[42] Inserting eq 3.4 into eq 2.1, we obtain the boson representation of the electron-transfer system

$$H = \frac{1}{2}\sum_{n,m} h_{nm}(X_nX_m + P_nP_m - \delta_{nm}) \tag{3.6}$$

As the mapping Hamiltonian (eq 3.6) contains only continuous operators, the quantum-mechanical system has a well-defined classical analogue. The transition to classical mechanics is performed by changing from the Heisenberg *operators* $y_k(t)$ ($y_k = X_n,P_n,x_j,p_j$) obeying Heisenberg's equations of motion ($i\dot{y}_k = [y_k,H]$) to the corresponding classical *functions* obeying Hamilton's equations (e.g., $\dot{X}_k = \partial H/\partial P_k$). In this classical limit, the formalism can be shown to recover the classical electron analogue model of Meyer and Miller.[32] To make contact with the mean-field trajectory method, the real-valued electronic variables X_n and P_n may be replaced by the complex-valued variables $d_n = (X_n + iP_n)/\sqrt{2}$, which have a similar meaning to the electronic coefficients in eq 3.1.[43] Although the equations of motion of both formulations are similar, the mapping formulation treats electronic and nuclear degrees of freedom on the same dynamical footing and is therefore superior to the mean-field trajectory method. The mapping formalism has been employed to facilitate the treatment of nonadiabatic dynamics in various theoretical approaches.[41,44−49] Furthermore, the formulation has been applied to a variety of systems with nonadiabatic dynamics,[43,50−53] including the description of photoinduced electron-transfer and internal-conversion processes.

To obtain the classical expectation value of an observable, say, the time-dependent diabatic population probability $P_2(t)$ defined in eq 2.3, the quantum-mechanical trace is replaced by a phase-space average

$$P_2(t) = \int \mathrm{d}\Gamma_0\, \rho(\Gamma_0)\, |d_2(t)|^2 \tag{3.7}$$

where Γ_0 denotes the trajectory $\Gamma_t = \{x_j(t),p_j(t),d_n(t)\}$ at $t = 0$ and $\rho(\Gamma_0)$ represents a phase-space distribution function describing the quantum-mechanical initial state of the system (see section 5.1 for details). To classically calculate adiabatic quantities, for example, the adiabatic population probability defined in eq 2.6, we use

$$P_2^{\mathrm{ad}}(t) = \int \mathrm{d}\Gamma_0\, \rho(\Gamma_0)\, |a_2(t)|^2 \tag{3.8}$$

where $a_n(t)$ are the electronic coefficients that are obtained when the total wave function is expanded in adiabatic basis states, that is, $|\Psi(t)\rangle = \sum_n a_n(t)|\psi_n^{\mathrm{ad}}\rangle$. By exploiting the unitary transformation between the diabatic and the adiabatic representation, the adiabatic coefficients $a_n(t)$ are readily obtained from the diabatic coefficients $d_n(t)$ and vice versa.[32,54]

IV. Classical Calculation of Electronic Spectra

In principle, we may use any of the above three methods (mean-field, surface hopping, and mapping) for a classical calculation of electronic spectra. In all formulations, the nonadiabatic dynamics of the molecular system are described by complex-valued variables $d_n(t)$ [or $a_n(t)$] for the electronic states and by the trajectory $\mathbf{x}(t)$ for the nuclear degrees of freedom. As derived in Appendix B, the classical limit of the pump−probe signal (eq 2.9) can be written in the form

$$I(t_\mathrm{d}) = \int \mathrm{d}\Gamma_0\, W(t_\mathrm{d})\, D(0)\, \rho(\Gamma_0) \tag{4.1}$$

where—in direct analogy to the quantum-mechanical expression—$D(0)$ and $W(t_\mathrm{d})$ are phase-space functions describing the pump and the probe processes. To calculate these functions, we introduce four classical approximations. The details of the derivations are given in Appendix B. The first three are based on the semiclassical Franck−Condon approximation,[7,8,30] which assumes that the Condon approximation holds (i.e., that μ_{nm} is coordinate-independent) and that we may employ a short-time approximation of the type $\mathrm{e}^{-ih_mt}\,\mathrm{e}^{ih_nt} \approx \mathrm{e}^{-i(V_m-V_n)t}$. The last formulation exploits the mapping transformation to directly calculate the dipole correlation function.[33]

A. First-Order Franck−Condon Approximation. The simplest way to generalize the standard Franck−Condon approximation to the case of vibronically coupled systems is to neglect the nonadiabatic coupling V_{12} during the duration of the short laser pulses. Doing so, we obtain for the classical doorway and window functions

$$D(0) = \frac{\mu^2}{4}\mathrm{e}^{-\alpha\tau_\mathrm{I}^2\{\omega_\mathrm{I}-[V_2(0)-V_0(0)]\}^2} \tag{4.2}$$

$$W(t_\mathrm{d}) = \frac{\mu^2}{4}\mathrm{e}^{-\alpha\tau_\mathrm{II}^2\{\omega_\mathrm{II}-[V_2(t_d)-V_0(t_d)]\}^2}\, |d_2(t_\mathrm{d})|^2 \tag{4.3}$$

Equations 4.1−4.3 offer a simple classical interpretation of time-resolved pump−probe spectroscopy, which becomes clear by outlining their numerical implementation: (i) Generate an ensemble of trajectories that represents the initial ground-state phase-space distribution $\rho(\Gamma_0)$ in eq 4.1. (ii) Because of the excitation of the system by a finite pump pulse at time $t = 0$, these trajectories are lifted to the optically allowed excited electronic state and are weighted in eq 4.2 by the resonance condition $\omega_\mathrm{I} = V_2(0) - V_0(0)$. (iii) Subsequently, the trajectories are propagated on the coupled excited electronic states, using some nonadiabatic classical method. (iv) At time $t = t_\mathrm{d}$, the contribution of each trajectory to the stimulated emission signal is given in eq 4.3 by the Gaussian factor describing time-dependent resonance condition $\omega_\mathrm{II} = V_2[x(t_\mathrm{d})] - V_1[x(t_\mathrm{d})]$ multiplied with electronic population probability $|d_2(t_\mathrm{d})|^2$ of the bright electronic state.

Equations 4.1−4.3 represent the simplest way to classically calculate pump−probe spectra. Obviously, it hardly requires

additional effort in the trajectory calculations. The nonadiabatic electron-transfer dynamics of the system enter through the time-dependent electronic population probability $|d_2(t_d)|^2$. In the absence of nonadiabatic coupling, the latter factor is constant and the above result becomes equivalent to previous results.[7−16] Because the underlying Franck−Condon approximation employs a short-time expansion of the propagator to the first order, the result will be referred to as the FC1 approximation.

B. Second-Order Franck−Condon Approximation. Using a short-time expansion that is valid in the second order,[55] the classical doorway and window functions can be derived as

$$D(0) = \frac{\mu^2}{4}\int_{-\infty}^{\infty} dt\, e^{-t^2/(2\alpha\tau_I^2)}\, e^{-\alpha\tau_I^2\{\omega_I-[V_2(t)-V_0(t)]\}^2} \quad (4.4)$$

$$W(t_d) = \frac{\mu^2}{4}\int_{-\infty}^{\infty} dt\, e^{-(t-t_d)^2/(2\alpha\tau_{II}^2)}\, e^{-\alpha\tau_{II}^2\{\omega_{II}-[V_2(t)-V_0(t)]\}^2}\, |d_2(t)|^2 \quad (4.5)$$

Similar to the first-order result, the second-order Franck−Condon (FC2) approximation accounts for the electron-transfer dynamics through the electronic population probability $|d_2(t_d)|^2$. In the absence of nonadiabatic coupling, eq 4.5 recovers the standard second-order results.[55] Interestingly, it is also equivalent to a semiclassical approximation of the Liouville von Neumann equation,[13,17] which has recently been generalized to the nonadiabatic case.[29] Besides the resonance conditions $\omega_i = V_2 - V_0$, the FC2 approximation also accounts for the time window $|\epsilon_i(t)|^2$ created by the laser pulses. Hence, the uncertainty relation between the time resolution (with respect to the delay time t_d) and the frequency resolution (with respect to the carrier frequencies ω_i) is correctly reproduced in the second order (but not by the first-order approximations 4.2 and 4.3).

The price to pay for this improvement is that we need to propagate classical trajectories during the interaction with the laser pulses. In the numerical implementation of the FC2 approximation, this raises the question whether the trajectories are propagated on the ground-state or excited-state potentials (in the quantum-mechanical formulation, the system propagates during interaction with the electric field in both electronic states according to the dipole operator $e^{-ih_m t}\mu_{mn}\, e^{ih_n t}$). The usual solution to this well-known ambiguity of the classical approximation is to choose the ground-state potential for the pump process and the excited-state potential for the probe process.[2]

While the latter works well for the calculation of the window function, the calculation of the doorway function requires some additional effort. This is because we also need to generate an appropriate excited-state phase-space distribution from the initial ground-state distribution $\rho(\Gamma_0)$. (Note that the FC1 approximation assumes that these two distributions are the same.) Converting the time integral in eq 4.4 into a sum

$$D(0) \propto \sum_j e^{-t_j^2/(2\alpha\tau_I^2)}\, e^{-\alpha\tau_I^2\{\omega_I-[V_2(t_j)-V_0(t_j)]\}^2} \quad (4.6)$$

we may consider the t_j's as "hopping times" at which the trajectories are lifted from the ground to the excited electronic state. This suggests the following scheme for the calculation of the doorway function: (i) For every trajectory of the initial ground-state phase-space distribution $\rho(\Gamma_0)$, we randomly select a hopping time t_j from their Gaussian distribution. (ii) For $t < t_j$, the trajectory is propagated on the ground-state potential. (iii) At $t = t_j$, the trajectory is lifted to the excited electronic state and weighted by the Gaussian resonance factor. For $t > t_j$, the trajectory is propagated on the excited-state potential.

C. Nonadiabatic Franck−Condon Approximation. Taking the vibronic coupling during the interaction with the laser pulses explicitly into account, Dilthey et al.[56] derived a generalization of the first-order Franck−Condon approximation to nonadiabatic systems. It leads to the classical doorway and window functions

$$D(0) = \frac{\mu^2}{4}\sum_{n=1,2} S_{2n}{}^2(0)\, e^{-2\alpha\tau_I^2\{\omega_I-[W_n(0)-V_0(0)]\}^2}$$

$$W(t_d) = \frac{\mu^2}{4}\sum_{n=1,2} S_{2n}{}^2(t_d)\, e^{-2\alpha\tau_{II}^2\{\omega_{II}-[W_n(t_d)-V_0(t_d)]\}^2}\, |a_n(t_d)|^2 \quad (4.7)$$

where the matrix **S** with elements

$$S_{2n}(t) = \sqrt{\frac{V_2(t)-V_1(t)}{2\sqrt{[V_2(t)-V_1(t)]^2 + V_{12}{}^2(t)}} + \frac{(-1)^n}{2}} \quad (4.8)$$

represents the unitary transformation between the diabatic and adiabatic representations.[37] In contrast to the approximations FC1 and FC2, which describe transitions between diabatic potentials, the Franck−Condon approximation including vibronic coupling (hereafter referred to as FCC) exhibits the adiabatic resonance conditions $\omega = W_n - V_0$. They account for transitions from both coupled adiabatic electronic potentials W_n to the electronic ground state V_0, which are weighted by its population probability $|a_n(t_d)|^2$. A further coordinate dependency arises from the prefactor $S_{2n}{}^2$, which represents the relation between the diabatic and the adiabatic energy gap. With respect to the short-time approximation of the propagator, eq 4.7 is a first-order expression and therefore suffers from the same shortcomings as eq 4.3.

D. Classical Dipole Function. Apart from the classical evaluation of the various Franck−Condon approximations, the mapping formulation provides an alternative approach to calculate the electronic dipole correlation function. The basic idea is to apply the mapping relation 3.4 directly to the electronic transition dipole operator, that is,

$$\hat{\mu}_{02}(t) = e^{iHt}|\psi_0\rangle\mu_{02}\langle\psi_2|\, e^{-iHt} \rightarrow \mu_{02}\frac{1}{2}[X_0(t) - iP_0(t)][X_2(t) + iP_2(t)] \equiv \mu_{02}(t) \quad (4.9)$$

This leads to the classical doorway and window functions

$$D(0) = \left|\int_{-\infty}^{\infty} dt\, \epsilon_1(t)\, \mu_{20}(t)\right|^2$$

$$W(t_d) = \left|\int_{-\infty}^{\infty} dt\, \epsilon_2(t)\, \mu_{02}(t)\right|^2 \quad (4.10)$$

As this expression was first introduced within the theoretical framework of the classical electron analogue model,[27,33] eq 4.10 will be referred to as the CEA approximation. Compared to approximations FC1, FC2, and FCC, which employ a classical method (e.g., mean-field, surface hopping, and mapping) to describe nonadiabatic dynamics *and* some type of Franck−Condon approximation, the CEA result (eq 4.10) only requires a single approximation, that is, the classical limit of the mapping relations (eq 3.4). A closer analysis shows that the structures of the CEA result (eq 4.10) and the FC2 result (eq 4.5) are quite similar in that both expressions are weighted by the diabatic population probability $|d_2|^2$ and account for the time window created by the laser pulse. In detail, however, the two expressions differ significantly.

E. Internal Transitions. In the optical spectroscopy of nonadiabatically coupled electronic states, two qualitatively different cases may occur: intramolecular and radiative couplings pertain to (a) *different* electronic transitions and (b) to the *same* electronic transitions. The two different situations are illustrated in Figure 1, which schematically shows two electron-transfer models with coupled electronic states $|\psi_1\rangle$ and $|\psi_2\rangle$. So far, we have been concerned with situation a, also referred to as the "external transition" case. In situation b, referred to as the "internal transition" case, we have the transition dipole operator

$$\hat{\mu} = |\psi_1\rangle\mu_{12}\langle\psi_2| + |\psi_2\rangle\mu_{21}\langle\psi_1| \tag{4.11}$$

which connects the coupled diabatic electronic states $|\psi_1\rangle$ and $|\psi_2\rangle$ (instead of $|\psi_0\rangle$ and $|\psi_2\rangle$ as in the external case).

Performing the derivations of the various classical approximations of the pump−probe signal for the internal case, there are only small changes for the Franck−Condon approximations FC1 and FC2. Because of the dipole operator in eq 4.11, the resonance factors in approximations 4.3 and 4.5 change to $\omega - (V_2 - V_1)$. Moreover, because both electronic states $|\psi_1\rangle$ and $|\psi_2\rangle$ are populated because of the vibronic coupling, in the internal case, the classical doorway and window functions describes both emission and absorption between these states. In the FC2 approximation, for example, we obtain

$$D(0) = \frac{\mu^2}{4}\int_{-\infty}^{\infty} \mathrm{d}t\, \mathrm{e}^{-t^2/(2\alpha\tau_I^2)}\, \mathrm{e}^{-\alpha\tau_I^2\{\omega_I-[V_2(t)-V_1(t)]\}^2}(|d_2(t)|^2 - |d_1(t)|^2)$$

$$W(t_d) = \frac{\mu^2}{4}\int_{-\infty}^{\infty} \mathrm{d}t\, \mathrm{e}^{-(t-t_d)^2/(2\alpha\tau_{II}^2)}\, e^{-\alpha\tau_{II}^2\{\omega_{II}-[V_2(t)-V_1(t)]\}^2} (|d_2(t)|^2 - |d_1(t)|^2) \tag{4.12}$$

and a similar result for the FC1 approximation.

Because the FCC approximation (eq 4.7) takes the nonadiabatic interaction during the radiative transitions explicitly into account, the results for the classical doorway and window functions differ in the external and internal cases.[56] In the latter, we obtain

$$D(0) = \frac{\mu^2}{4}\left[S_{22}{}^2(0) - \frac{1}{2}\right] \mathrm{e}^{-2\alpha\tau_I^2\{\omega_I-[W_2(0)-W_1(0)]\}^2}$$

$$W(t_d) = \frac{\mu^2}{4}\left[S_{22}{}^2(t_d) - \frac{1}{2}\right] \mathrm{e}^{-2\alpha\tau_{II}^2\{\omega_{II}-[W_2(t_d)-W_1(t_d)]\}^2} (|a_2(t_d)|^2 - |a_1(t_d)|^2) \tag{4.13}$$

In the CEA approximation for the internal case, we obtain the classical dipole function $\mu_{12}(t)$ instead of $\mu_{02}(t)$ in eq 4.10. As shown in the Appendix, this gives rise to a population term $|d_2(t)|^2 \cdot |d_1(t)|^2$ instead of the population difference obtained in eq 4.12. In practice, however, it has proven advantageous to consider emission and absorption separately, see eq B7.

F. Ground-State Contribution. Besides the excited-state contribution discussed so far, the transient absorption spectrum also contains contributions from the electronic ground state. On one hand, the reduced population in the electronic ground state causes a bleach of the absorption band, which is obtained by calculating the linear absorption of the probe pulse (e.g., at the FC1 level, the bleach signal is $\propto \mathrm{e}^{-\alpha\tau_{II}^2\{\omega_{II}-[V_2(0)-V_0(0)]\}^2}$). On the other hand, finite pump pulses give rise to stimulated impulsive Raman scattering.[2,40] As shown in Appendix A, this ground-state contribution can also be cast in doorway−window expression 2.9 and contains the Liouville operators given in eq A6. A simple classical approximation of the latter can be derived as follows.

Let us first consider the first-order short-time approximation to the ground-state doorway operator

$$\mathscr{D}_g\rho_0 = \mu^2\int_{-\infty}^{\infty} \mathrm{d}t_2\, \epsilon_I(t_2)\, \mathrm{e}^{-i(V_2-V_0)t_2} \times \int_{-\infty}^{t_2} \mathrm{d}t_1\, \epsilon_I(t_1)\, \mathrm{e}^{i(V_2-V_0)t_1}\, \langle\psi_0|\rho_0|\psi_0\rangle\, |\psi_0\rangle\langle\psi_0| \tag{4.14}$$

where the electronic projector states that the molecular system evolves in the electronic ground state after the interaction with the pump field. Although the expression formally looks quite similar to the corresponding doorway operator for the excited-state contribution, its further evaluation is more cumbersome because of the time ordering of the integrals. To obtain a simple and computationally convenient classical expression for the ground-state contribution, we choose to simply ignore the time ordering (i.e., we shift the upper integral limit from t_2 to ∞). Then, the classical evaluation is straightforward and yields the FC1 approximation $D_g(0) = {}^{\mu^2}/_4\, \mathrm{e}^{-\alpha\tau_I^2\{\omega_I-[V_2(0)-V_0(0)]\}^2}$. Apart from the fact that the trajectories evolve in the electronic ground state after the interaction with the pump field, the latter is identical to the excited-state expression (eq 4.2). Ignoring the integral time ordering in the second-order expansion (eq B2), we obtain the FC2 approximation of the ground-state contribution

$$D_g(0) = \frac{\mu^2}{4}\int_{-\infty}^{\infty} \mathrm{d}t\, \mathrm{e}^{-t^2/(2\alpha\tau_I^2)}\, \mathrm{e}^{-\alpha\tau_I^2\{\omega_I-[V_2(t)-V_0(t)]\}^2} \tag{4.15}$$

$$W_g(t_d) = \frac{\mu^2}{4}\int_{-\infty}^{\infty} \mathrm{d}t\, \mathrm{e}^{-(t-t_d)^2/(2\alpha\tau_{II}^2)}\, \mathrm{e}^{-\alpha\tau_{II}^2\{\omega_{II}-[V_2(t)-V_0(t)]\}^2}\, |d_0(t)|^2 \tag{4.16}$$

which again looks quite similar to the corresponding excited-state expressions 4.4 and 4.5. Note that the molecular system

evolves in the electronic ground state between the interaction with two laser pulses, while it evolves in the excited electronic state during the pulses.

The ground-state doorway function (eq 4.15) can be evaluated using the following scheme. (i) For every trajectory of the initial ground-state phase-space distribution $\rho(\Gamma_0)$, we randomly select two hopping times t_a and t_b from the Gaussian distribution $e^{-t2/(2\alpha\tau_1^2)}$, for which we require that $t_a < t_b$. (ii) For $t < t_a$, the trajectory is propagated on the ground-state potential. (iii) When the trajectory to the excited electronic state at $t = t_a$ is lifted, the trajectory is weighted by the Gaussian resonance factor and is propagated on the excited-state potential for $t_a < t < t_b$. (iv) At $t = t_b$, the trajectory is moved back to the ground-state potential and propagates in the electronic ground state until the arrival of the probe laser field. Then, the ground-state window function (eq 4.16) is evaluated in a similar manner.

V. Computational Results

A. Computational Details. The computational methods employed for the quantum-mechanical wave packet propagations have been described in detail in ref 20. In short, the time-dependent Schrödinger equation is converted into a numerically tractable problem by expanding the state vector in a direct-product basis constructed from diabatic electronic states and harmonic-oscillator states for the vibrational degrees of freedom. This results in a system of coupled first-order differential equations, which are solved using a Runge−Kutta−Merson scheme with an adaptive step size. The quantum-mechanical transient absorption spectrum (eq 2.9) has been calculated (numerically) exactly by using a nonperturbative evaluation of the electronic polarization.[20,57]

The classical mapping method and its numerical implementation have been described in refs 26 and 41. Basically, Hamilton's equations pertaining to the classical Hamiltonian (eq 3.6) are solved for the electronic (X_n, P_n) and nuclear (x_j, p_j) degrees of freedom, using again a Runge−Kutta−Merson integrator. To calculate quasiclassical averages $\int d\Gamma\rho(\Gamma)...$ (as, e.g., in eq 3.7), the quantum-mechanical initial state $\rho_0 = \rho_{el}\rho_{vib}$ is to be represented by a suitable phase-space distribution $\rho(\Gamma)$. In this work, the vibrational system was assumed to be in its harmonic ground state, $\rho_{vib} = |0\rangle\langle 0|$, which was represented by a Wigner distribution.[8] Within the mapping formalism, the electronic initial state $\rho_{el} = |\psi_0\rangle\langle\psi_0|$ is mapped onto the harmonic-oscillator eigenstate $|1_0 0_1 0_2\rangle$ containing a single quantum excitation in the first mode [see eq 3.5]. As is well-known, the Wigner distribution of the latter state is not positive-definite and therefore is problematic in a quasiclassical implementation. We therefore change to classical action-angle variables $\{N_n, Q_n\}$ using the transformations $X_n = \sqrt{2N_n+1}\sin Q_n$ and $P_n = \sqrt{2N_n+1}\cos Q_n$, sample the angles Q_n from $[0, 2\pi]$, and fix the actions N_n to represent the quantum number of the oscillator.[26] This yields

$$\rho_{el}(N_1,N_2) = \delta\left(N_1 - \frac{1}{2}\right)\delta\left(N_2 - \frac{3}{2}\right) \qquad (5.1)$$

where the factors $^1/_2$ reflects the zero-point energy of the harmonic oscillators. Converged quasiclassical averages for the time-resolved signals (e.g., as in Figure 2) and for time- and frequency-resolved spectra (e.g., as in Figure 3) are obtained by running 10^4 trajectories.

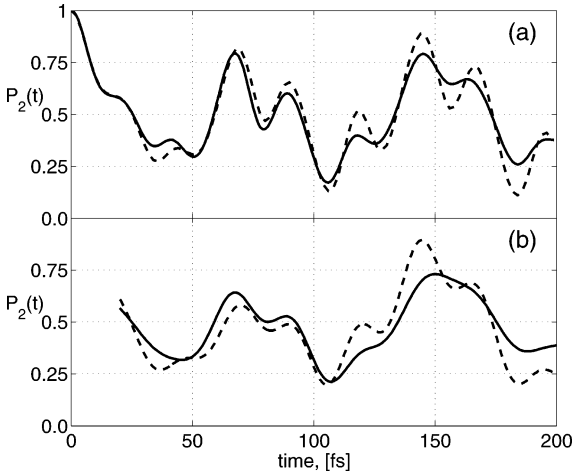

Figure 2. Time-dependent population $P_2(t)$ of the optically excited diabatic electronic state, as obtained for the one-mode electron-transfer model. Compared are classical mapping results (solid lines, eq 3.7) and quantum-mechanical reference calculations (dashed line, eq 2.3) for the cases of (a) impulsive excitation and (b) excitation by a Gaussian pump pulse of 20 fs duration (shown only for $t > 25$ fs, i.e., after the pump pulse).

B. One-Mode Three-State Model. To consider the case of external radiative transitions, we adopt the one-mode three-state model proposed in ref 45, which comprises an energetically well-separated electronic ground state $|\psi_0\rangle$ and two nonadiabatically coupled excited states $|\psi_1\rangle$ and $|\psi_2\rangle$. The parameters of the model are $E_0 = -1.775$ eV, $E_1 = E_2 = 0$, $g = 0.05$ eV, $\omega = g$, $\kappa^{(0)} = -3g$, and $\kappa^{(2)} = -\kappa^{(1)} = g/2$. The diabatic potential-energy curves $V_n(x)$ of the model are shown in Figure 1a.

In a first step, it is instructive to study the quantum-mechanical electron-transfer dynamics of the system. To this end, Figure 2a shows the population probability $P_2(t)$ (see eq 2.3) of the diabatic electronic state $|\psi_2\rangle$. As schematically indicated in Figure 1a, it is assumed that at time $t = 0$ this state is impulsively excited by an ultrashort laser pulse. Following an ultrafast initial decay, the quantum-mechanical result for $P_2(t)$ is seen to exhibit quasiperiodic oscillations with periods of ≈24 and 70 fs. A closer analysis shows that these dynamics are caused by the two shortest vibronic periodic orbits of the system.[34,45]

To further illustrate the motion of the laser-induced wave packet on the coupled potential-energy curves V_1 and V_2, Figure 3 shows the time-dependent probability distribution $P_2(x,t)$ defined in eq 2.4. As a consequence of the impulsive $|\psi_0\rangle \rightarrow |\psi_2\rangle$ excitation, the wave function at time $t = 0$ is a Gaussian centered at $x_0 = 3$. With increasing time, the wave packet is seen to undergo oscillations along x with a period of ≈ 70 fs, which roughly corresponds to the vibrational frequency ω of the model. Note that the nuclear motion is directly linked to an oscillation of the electronic population; that is, the vibrational dynamics trigger electronic transitions between the two coupled states $|\psi_1\rangle$ and $|\psi_2\rangle$.[58]

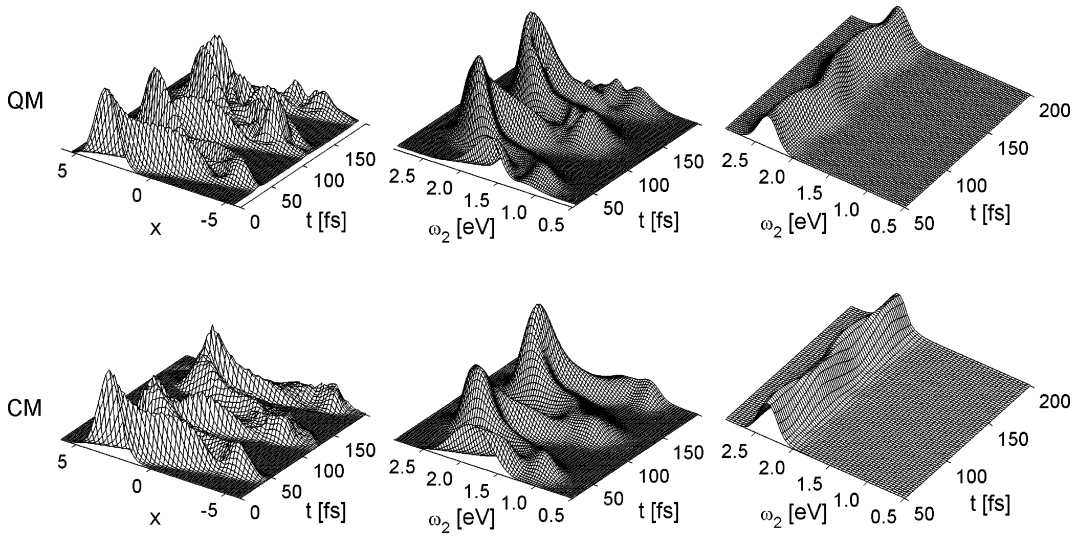

Figure 3. Comparison of the quantum-mechanical (QM, upper panels) and classical (CM, lower panels) electron-transfer dynamics and spectroscopy of the one-mode model. Shown are (left) the time-dependent nonadiabatic wave packet motion as described by the probability density $P_2(x,t)$ in eq 2.4 as well as the excited-state (stimulated emission, middle) and the ground-state (impulsive Raman scattering, right) contributions to the transient absorption spectrum. The classical spectra are calculated using the FC2 approximation in eqs 4.5 and 4.16.

We now turn to the classical mapping calculation for the one-mode three-state model. As discussed before,[58] the nonadiabatic quantum dynamics of the system are nicely reproduced by the classical formulation. While we find almost quantitative agreement of the classical and quantum-mechanical diabatic populations in Figure 2a, the comparison of the corresponding time-dependent probability distributions $P_2(x,t)$ in Figure 3 reveals the limits of the classical approximation. Although the mapping calculation catches the main features of the nonadiabatic wave packet motion, it is seen to miss the finer details and substructures at longer times.

It is interesting to study to what extent the electron-transfer dynamics are reflected in the excited-state contribution to the transient absorption spectrum. Assuming impulsive excitation and probe pulses of 20 fs duration, Figure 3 shows the quantum-mechanical pump−probe signal as a function of the delay time t_d and the probe carrier frequency ω_{II}. As discussed by several authors,[9,40,59] the excited-state pump−probe signal nicely maps the time evolution of the quantum-mechanical wave function. To obtain a first impression on the overall performance of a classical description, Figure 3 also shows the corresponding transient absorption signal as obtained from the second-order Franck−Condon approximation (eq 4.5). As in the case of the wave packet dynamics discussed above, the classical transient absorption spectrum is in excellent agreement with the quantum reference calculation for times up to 150 fs. Only at longer times, the classical description deteriorates and fails to resolve the finer details of the spectrum.

We are now in a position to study the accuracy of the various classical approximations to the transient absorption introduced above, that is, the Franck−Condon approximation to first-order (FC1), second-order (FC2), and vibronic coupling (FCC), as well as the classical electron analogue model (CEA) approximation. To this end, Figure 4 shows cuts of the above-discussed transient absorption spectrum

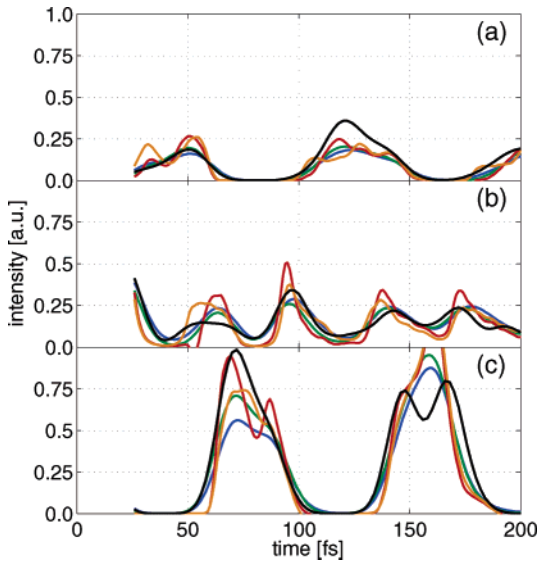

Figure 4. Cuts of the excited-state contribution to the transient absorption spectrum at probe carrier frequencies (a) 1.25 eV, (b) 1.75 eV, and (c) 2.25 eV, obtained for the one-mode electron-transfer model. The classical approximations FC1 (red lines, eq 4.3), FC2 (green lines, eq 4.5), FCC (orange lines, eq 4.7), and CEA (blue lines, eq 4.10) are compared to exact quantum calculations (black lines).

at probe carrier frequencies ω_{II} = (a) 1.25 eV, (b) 1.75 eV, and (c) 2.25 eV, corresponding to the low-, middle- and high-frequency regions, respectively, of the spectrum shown in Figure 3. While all classical approximations account for the time evolution of the spectrum at least qualitatively, clear differences are observed. First, we note that the two first-order approximations FC1 and FCC may give rise to spurious structures of the time-resolved signal, which indicate that these approximations fail to correctly account for the averaging effect caused by finite pulses. Although the FCC description clearly represents an improvement over the simple FC1 approximation, its higher computational effort

compared to the FC1 and FC2 calculations renders this method less attractive.

The FC2 (eq 4.5) and the CEA (eq 4.10) classical descriptions, on the other hand, are clearly superior to the first-order approximations. Considering that their derivations are based on quite different assumptions, the two formulations give surprisingly similar results, at least for the simple model under consideration. Their main deviation from the quantum calculation—the failure to reproduce the dip of the pump−probe signal at 2.25 eV—is caused by the limits of the classical mapping calculations (it already shows up in the classical wave packet calculation in Figure 3) and not by the approximate calculation of the spectrum.

So far, we have restricted the discussion to the case of impulsive excitation ($\tau_I = 0$). To study the effect of finite pump pulses on the electron-transfer dynamics, Figure 2b shows the diabatic population $P_2(t)$ in the case of a resonant ($\omega_I = E_2 - E_0$) pump pulse of 20 fs duration. As is expected, the finite pulse tends to smear out the time evolution of electronic population dynamics. When the FC2 doorway function (eq 4.4) is used, the corresponding classical calculation is seen to somewhat exaggerate this broadening effect, particularly at longer times. Because the latter also occurs in the case of impulsive excitation, it again seems to be caused less by the approximate calculation of the doorway function rather than by the approximate calculation of the nonadiabatic dynamics through the classical mapping calculations.

Finally, we wish to study the performance of the classical approximation to calculate the ground-state contribution to the transient absorption spectrum. Employing the FC2 ground-state doorway and windows functions 4.15 and 4.16, Figure 3 compares quantum and classical results of the time-resolved ground-state pump−probe signal, sometimes referred to as "impulsive stimulated Raman" emission.[40] As the name indicates, the ground-state contribution mainly reflects vibrational dynamics in the electronic ground state and therefore yields only little information on the excited-state electron-transfer dynamics. The coherent vibrational motion seen in the quantum calculation is nicely reproduced by the classical results.

C. Three-Mode Two-State Model. To describe the situation of internal radiative transitions, we consider a two-state three-mode system describing the photoinduced electron-transfer process of the mixed-valence system $(NH_3)_5Ru^{III}NCRu^{II}(CN)_5^-$ investigated by Barbara and coworkers.[60] On the basis of the model of Wang and Thoss,[35] we choose the parameters (in eV) $E_1 = 0$, $E_2 = 1.177$, $g = 0.186$, $\omega_1 = 0.2615$, $\omega_2 = 0.0565$, $\omega_3 = 0.0198$, $\kappa_n^{(1)} = 0$, $\kappa_1^{(2)} = 0.2003$, $\kappa_2^{(2)} = 0.1474$, and $\kappa_3^{(2)} = 0.0496$. The diabatic potential-energy curves $V_n(x_2)$ of the model along the most important vibrational mode x_2 are shown in Figure 1b.

Assuming again that the diabatic electronic state $|\psi_2\rangle$ is impulsively excited at time $t = 0$, Figure 5a shows the quantum-mechanical diabatic population probability $P_2(t)$ of the two-state three-mode model. The diabatic population is seen to exhibit a complex stepwise decay within the first ≈200 fs. Also shown in Figure 5b is the adiabatic population probability $P_2^{ad}(t)$ (see eq 2.6), which is surprisingly similar to the diabatic population $P_2(t)$. Unlike the simple one-mode model discussed above, however, the coupling between the electronic and the vibrational dynamics is not as straightforward for the three-mode model. As an example, Figure 6 shows the time-dependent probability densities $P_2(x_2,t)$ and $P_1(x_2,t)$, reflecting the time evolution of the nonadiabatic wave packet motion on the diabatic electronic states $|\psi_2\rangle$ and $|\psi_1\rangle$, respectively. (For brevity, we restrict the discussion to the coordinate x_2, which represents the most important vibrational mode of the model.) Starting at time $t = 0$ in the upper electronic state at position $x_2 = 0$, the wave packet reaches the crossing region within ≈20 fs and bifurcates into two components evolving on the two coupled electronic surfaces. The excited-state component of the wave packet is seen to decay within a few hundred femtoseconds, while in the electronic ground-state potential, the vibrational motion is only weakly damped.

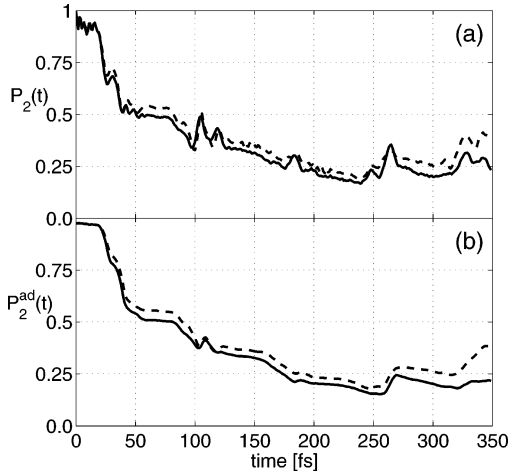

Figure 5. Time evolution of the electronic population probability of the (a) diabatic and (b) adiabatic optically excited electronic state. Compared are classical mapping results (solid lines, eqs 3.7 and 3.8) and quantum-mechanical reference calculations (dashed lines, eqs 2.3 and 2.6), as obtained for the three-mode electron-transfer model.

Let us turn to the transient absorption spectrum of the three-mode model. As the ground-state contribution essentially reflects simple harmonic vibrational motion similar to the one-mode case, we restrict the discussion to the excited-state contribution to the spectrum shown in Figure 6. The three-mode model is seen to give rise to pronounced wave packet motion, exhibiting stimulated emission ($I > 0$) as well as transient absorption ($I < 0$) from the hot ground state. We note that the latter reflects parts of the wave packet that decayed via the curve crossing to the electronic ground state. The wave packet dynamics mostly reflects the motion along the x_2 coordinate, which is strongly shifted ($\kappa_2^{(2)}/\omega_2 \approx 1$) and shows a period of $T_{\omega_2} \approx 70$ fs. This is because the high-frequency vibration ω_1 ($T_{\omega_1} \approx 16$ fs) is too fast to be resolved by 20 fs pulses, and the low-frequency vibration ω_3 ($T_{\omega_3} \approx 200$ fs) is quite slow on the time scale considered and only affects a minor overall widening of the spectrum around ≈200 fs.

Finally, we wish to consider the performance of various classical models. To this end, Figures 5 and 6 compare the

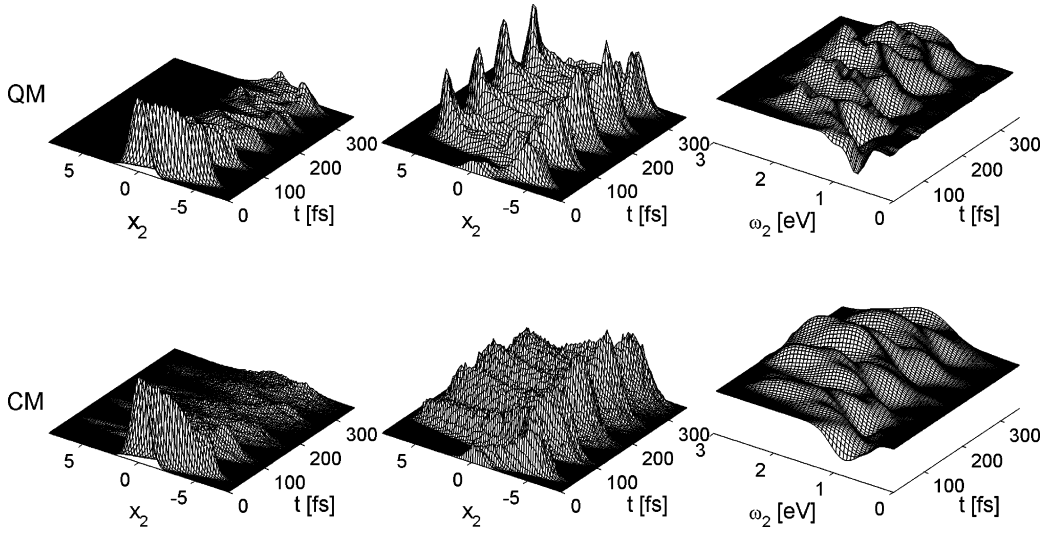

Figure 6. Comparison of the quantum-mechanical (QM, upper panels) and classical (CM, lower panels) electron-transfer dynamics and spectroscopy of the three-mode model. Shown are the time-dependent nonadiabatic wave packet motion as described by the probability densities (left) $P_2(x_2,t)$ and (middle) $P_1(x_2,t)$ (eq 2.4), as well as (right) the excited-state contribution to the transient absorption spectrum. The classical spectrum is calculated using the FC2 approximation in eq 4.5.

quantum and classical electronic population probabilities and probability densities, respectively. The simple classical mapping formulation model is seen to reproduce the complex structures of the electronic populations and the nonadiabatic wave packet motion with surprising accuracy. The classical calculation only misses fine details of the vibrational structures, such as the complete rephasing of the wave packet at the turning point of the potential at $x_2 \approx 5$. Similarly, the classical transient absorption spectrum calculated at the FC2 level is found to be in excellent agreement with the quantum result. The only difference to be seen in Figure 6 is that the classical spectrum reaches somewhat further toward the high-frequency side.

To study the accuracy of the various classical approximations to the transient absorption for the three-mode model, Figure 7 shows cuts of the transient absorption spectrum at probe carrier frequencies (a) 1.0 eV, (b) 1.5 eV, and (c) 2.0 eV. Again, it is found that the two first-order approximations FC1 and FCC give rise to spurious structures of the time-resolved signal, which indicate that these approximations fail to correctly account for the averaging effect caused by finite pulses. The FC2 and the CEA approximations are found to be quite similar and give a fairly accurate description of the transient absorption spectrum of the three-mode model.

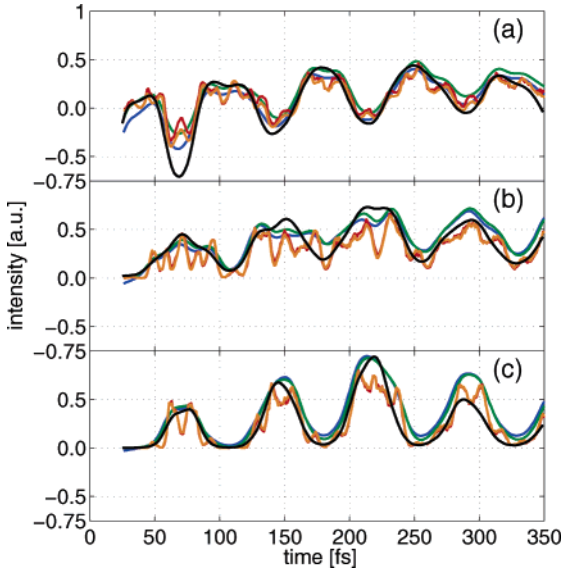

Figure 7. Cuts of the excited-state contribution to the transient absorption spectrum at probe carrier frequencies (a) 1.0 eV, (b) 1.5 eV, and (c) 2.0 eV, obtained for the three-mode electron-transfer model. The classical approximations FC1 (red lines, eq 4.3), FC2 (green lines, eq 4.5), FCC (orange lines, eq 4.13), and CEA (blue lines, eqs 4.10 and B7) are compared to exact quantum calculations (black lines).

VI. Conclusions

We have outlined a classical approach to the calculation of time- and frequency-resolved pump−probe spectra of nonadiabatically coupled molecular systems. We have generalized the first- and second-order semiclassical Franck−Condon approximations to the case of vibronically coupled potential-energy surfaces (FC1 and FC2), proposed a classical version of a nonadiabatic version of the Franck−Condon approximation (FCC), and employed a classical analogue of the electronic dipole function (CEA). When established models describing ultrafast photoinduced electron transfer are adopted,[34,35] it has been found that the two first-order approximations FC1 and FCC give rise to spurious structures of the time-resolved signal, which indicate that these approximations fail to correctly account for the averaging effect caused by finite pulses. The FC2 and CEA approximations, on the other hand, were found to be quite similar and gave a fairly accurate description of the transient absorption spectrum of the electron-transfer models under consideration. As the numerical implementation of the derived doorway and window functions at the FC2 level (eqs 4.4 and 4.5) is rather straightforward, the generalized second-order Franck−Condon approximation appears to be the method of choice.

Apart from the excited-state contribution for which a

number of classical formulations has been proposed, we have also considered the classical evaluation of the ground-state contribution to the transient absorption spectrum. Although additional assumptions need to be invoked in order to implement the FC2 approximation for this case, the resulting classical calculations compare well to the quantum reference results. Furthermore, we have devised a practical scheme (eq 4.6) to account for effects of pump pulses of finite duration.

Throughout this paper, we have employed the mapping approach in order to achieve a classical description of nonadiabatic quantum dynamics. The classical limit of the mapping formulation has been shown to work surprisingly well for the electron-transfer models under consideration. Nevertheless, the derivations of the various classical approximations are by no means restricted to the mapping formulation but can be used as well by employing other classical models of nonadiabatic quantum dynamics, such as the mean-field trajectory or the surface-hopping method.

Acknowledgment. We thank Michael Thoss for numerous inspiring and helpful discussions. This work has been supported by the Frankfurt Center for Scientific Computing, the Fonds der Chemischen Industrie, and the Deutsche Forschungsgemeinschaft.

Appendix A: Quantum Description

Considering the external case defined by eqs 2.1 and 2.7, we wish to derive the quantum-mechanical result for the pump−probe signal (eq 2.9). Prior to the interaction with the laser field, we assume that the system is in its electronic and vibrational ground state $|\Psi_0\rangle = |\psi_0\rangle|\phi_0\rangle$. When time-dependent perturbation theory is employed with respect to the field-matter interaction, the wave function after the interaction with the pump field can be written as[2]

$$|\Psi_A\rangle = i\int_{-\infty}^{\infty} dt'\, \epsilon_1(t')\, \hat{\mu}(t')|\Psi_0\rangle \equiv A\,|\Psi_0\rangle \qquad (A1)$$

where the operator A accounts for the $|\psi_0\rangle \rightarrow |\psi_2\rangle$ absorption process and $\hat{\mu}(t) = e^{iHt}\,\hat{\mu}\,e^{-iHt}$ represents the transition dipole operator in the Heisenberg representation. Similarly, the wave function after the interaction with the second pulse reads

$$|\Psi_{EA}\rangle = i\int_{-\infty}^{\infty} dt'\, \epsilon_2(t')\, \hat{\mu}(t')|\Psi_A\rangle \equiv E|\Psi_A\rangle \qquad (A2)$$

Assuming that the measured pump−probe signal is directly proportional to the field-induced population in the final electronic state, the excited-state spectroscopic signal is given by

$$I = \langle\Psi_A|E^{\dagger}E|\Psi_A\rangle$$
$$= \int_{-\infty}^{\infty} dt_2 \int_{-\infty}^{\infty} dt_1\, \epsilon_2(t_2)\, \epsilon_2(t_1)\langle\Psi_A|\hat{\mu}(t_1)\,\hat{\mu}(t_2)|\Psi_A\rangle \qquad (A3)$$

When the initial density operator $\rho_0 = |\Psi_0\rangle\langle\Psi_0|$ is introduced, this can be rewritten as

$$I = \mathrm{Tr}\{A\,e^{-iHt}\,E\rho_0E^{\dagger}\,e^{iHt}\,A^{\dagger}\} \qquad (A4)$$

$$= \mathrm{Tr}\{\mathscr{W}e^{-i\mathscr{L}t_d}\mathscr{D}\rho_0\} \qquad (A5)$$

where we defined the Liouville operators $\mathscr{D}\rho = A\rho A^{\dagger}$, $\mathscr{L}\rho = [H,\rho]$, and $\mathscr{W}\rho = E\rho E^{\dagger}$ to recover the doorway−window expression in eq 2.9.

Similarly, the ground-state signal (because of impulsive stimulated Raman scattering) discussed in section IV.F is obtained by projecting the fourth-order wave function $|\Psi_{EAEA}\rangle$ on the initial state $|\Psi_0\rangle$.[2] The resulting expression can be cast in doorway−window form (eq A5) with the Liouville operators

$$\mathscr{D}_g = E^{\dagger}A = \int_{-\infty}^{\infty} dt_2 \int_{-\infty}^{t_2} dt_1\, \epsilon_I(t_2)\, \epsilon_I(t_1)\, \hat{\mu}(t_2)\, \hat{\mu}(t_1)$$

$$\mathscr{W}_g = E^{\dagger}A = \int_{-\infty}^{\infty} dt_2 \int_{-\infty}^{t_2} dt_1\, \epsilon_{II}(t_2)\, \epsilon_{II}(t_1)\, \hat{\mu}(t_2)\, \hat{\mu}(t_1) \qquad (A6)$$

Note that because of eq A6 the molecular system evolves in the electronic ground state between the interaction with two laser pulses, while in eq A4, the system evolves in the excited electronic state between pulses.

Appendix B: Classical Approximations

To derive the FC1 result (eq 4.2), we employ the first-order short-time approximation $e^{-ih_m t}\,e^{ih_n t} \approx e^{-i(V_m - V_n)t}$ to the Heisenberg dipole operator $\hat{\mu}(t)$.[7,8,30] This allows us to perform the time integrations in eq A3 and yields for the doorway and window operators

$$\mathscr{D}\rho_0 = \frac{\mu^2}{4}\, e^{-\alpha\tau_I^2[\omega_1-(V_2-V_0)]^2}\langle\psi_0|\rho_0|\psi_0\rangle\,|\psi_2\rangle\langle\psi_2|$$

$$\mathscr{W} = \frac{\mu^2}{4}\, e^{-\alpha\tau_{II}^2[\omega_{II}-(V_2-V_0)]^2}|\psi_2\rangle\langle\psi_2| \qquad (B1)$$

By replacing the quantum-mechanical trace in eq A5 by the classical phase-space average $\int d\Gamma_0 ...$ defined in eq 3.7, the classical limit of the doorway−window expression (eq A5) is given by eq 4.1 with the classical doorway and window functions of eq 4.2.

When the second-order short-time approximation[55] is employed,

$$e^{ih_2t_1}\,\mu_{20}\,e^{ih_0(t_2-t_1)}\,\mu_{02}\,e^{ih_2t_2} \approx$$
$$e^{ih_2(t_2-t_1)/2}\,\mu_{20}\,e^{i(V_2-V_0)(t_2-t_1)}\,\mu_{02}\,e^{ih_2(t_2-t_1)/2} \qquad (B2)$$

only one of the two time integrations in eq A3 can be performed analytically. This yields the window operators[55]

$$\mathscr{W} = \frac{\mu^2}{4}\int_{-\infty}^{\infty} dt\, e^{-(t-t_d)^2/(2\alpha\tau_{II}^2)}\, e^{-\alpha\tau_{II}^2[\omega_{II}-(V_2-V_0)]^2}|\psi_2\rangle\langle\psi_2| \qquad (B3)$$

and a similar result for the doorway operator. In the classical limit, we obtain the FC2 result (eq 4.5).

Assuming that the matrix elements of the diabatic Hamiltonian commute (i.e., $[h_{nm}, h_{kl}] = 0$), Dilthey et al.[56] performed a resummation of the Heisenberg dipole operator expansion, which leads to closed expressions for the spectroscopic projection operators A (eq A1) and E (eq A2). In the external case, one obtains for the window operator

$$\mathscr{W} = \frac{\mu^2}{4}\sum_{n=1,2} {S_{2n}}^2\, e^{-2\alpha\tau_{II}^2[\omega_{II}-(W_n-V_0)]^2}|\psi_n^{ad}\rangle\langle\psi_n^{ad}| - \frac{\mu^2}{4} e^{-\alpha\tau_{II}^2\{[\omega_{II}-(W_2-V_0)]^2+[\omega_{II}-(W_1-V_0)]^2\}}\left({S_{22}}^2-\frac{1}{2}\right)(|\psi_1^{ad}\rangle\langle\psi_2^{ad}| + \text{h.c.}) \quad \text{(B4)}$$

where $|\psi_n^{ad}\rangle$ and W_n denote adiabatic states and potentials, respectively, defined in eq 2.5, and the matrix $\{S_{mn}\}$ is given in eq 4.8. Containing two resonance conditions, the last term in eq B4 is usually strongly suppressed and can be omitted. In the classical limit, the FCC result (eq 4.7) is recovered. In the internal case, we obtain[56]

$$\mathscr{W} = \frac{\mu^2}{4}\left({S_{22}}^2-\frac{1}{2}\right)^2 e^{-2\alpha\tau_{II}^2[\omega_{II}-(W_2-W_1)]^2}(|\psi_2^{ad}\rangle\langle\psi_2^{ad}| - |\psi_1^{ad}\rangle\langle\psi_1^{ad}|) \quad \text{(B5)}$$

where again off-resonant terms have been neglected. In the classical limit, this yields eq 4.13.

The CEA result (eq 4.10) is directly obtained from eq A3 by employing the classical mapping of the electronic transition dipole operator in eq 4.9. The calculation is straightforward in the external case.[27] In the internal case, we recall that the quantum-mechanical pump−probe signal consists of two contributions, reflecting absorption and emission between the coupled electronic states $|\psi_1\rangle$ and $|\psi_2\rangle$. In the CEA formulation, we also obtain two terms, $\mu_{12}(t) + \mu_{21}(t)$, which, however, collapse to the term $2Re\mu_{21}(t)$ within approximation 4.9. Hence, in the internal case, both absorption and emission are described by a single dipole function and therefore in an averaged manner.

To motivate a way to improve upon this simple approximation, we change to classical action angle variables via $\sqrt{N_n}\, e^{iQ_n} = (X_n + iP_n)/\sqrt{2}$,[32] thus obtaining for the mapped transition dipole function[33]

$$\mu_{12}(t) = \mu\sqrt{\left(N_1+\frac{1}{2}\right)\left(N_2+\frac{1}{2}\right)}\, e^{i(Q_2-Q_1)} \quad \text{(B6)}$$

A simple way to consider absorption and emission separately is to replace the CEA dipole functions in eq B6 by

$$\tilde{\mu}_{12}(t) = \mu_{12}\sqrt{\left(N_2+\frac{1}{2}\right)}\, e^{i(Q_2-Q_1)}$$

$$\tilde{\mu}_{21}(t) = \mu_{21}\sqrt{\left(N_1+\frac{1}{2}\right)}\, e^{i(Q_1-Q_2)} \quad \text{(B7)}$$

where now—as in the quantum case—the emission term depends on the excited-state population N_2 and the absorption term on the ground-state population N_1.

References

(1) Zewail, A. H. *J. Phys. Chem. A* **2000**, *104*, 5660−5694.

(2) Mukamel, S. *Principles of Nonlinear Optical Spectroscopy*; University Press: Oxford, U. K., 1995.

(3) Domcke, W.; Yarkony, D. R.; Köppel, H. *Conical Intersections*: *Electronic Structure*, *Dynamics and Spectroscopy*; World Scientific: Singapore, 2004.

(4) Ben-Nun, M.; Quenneville, J.; Martínez, T. J. *J. Phys. Chem. A* **2000**, *104*, 5161−5175.

(5) Doltsinis, N. L.; Marx, D. *J. Theor. Comput. Chem.* **2002**, *1*, 319−349.

(6) Carloni, P.; Rothlisberger, U.; Parrinello, M. *Acc. Chem. Res.* **2002**, *35*, 455−464.

(7) Mukamel, S. *J. Chem. Phys.* **1982**, *77*, 173−181.

(8) Schinke, R. *Photodissociation Dynamics*; University Press: Cambridge, U. K., 1993.

(9) Braun, M.; Meier, C.; Engel, V. *J. Chem. Phys.* **1995**, *103*, 7907−7911.

(10) Braun, M.; Meier, C.; Engel, V. *J. Chem. Phys.* **1996**, *105*, 530−534.

(11) Meyer, S.; Meier, C.; Engel, V. *J. Chem. Phys.* **1998**, *108*, 7631−7636.

(12) Zadoyan, R.; Li, Z.; Martens, C. C.; Apkarian, V. A. *J. Chem. Phys.* **1994**, *101*, 6648−6657.

(13) Li, Z.; Fang, J.-Y.; Martens, C. C. *J. Chem. Phys.* **1996**, *104*, 6919−6929.

(14) Sterling, M.; Zadoyan, R.; Apkarian, V. A. *J. Chem. Phys.* **1996**, *104*, 6497−6506.

(15) Ungar, L. W.; Cina, J. A. *Adv. Chem. Phys.* **1997**, *100*, 171−228.

(16) Shen, Y.-C.; Cina, J. A. *J. Chem. Phys.* **1999**, *110*, 9793−9806.

(17) Hartmann, M.; Pittner, J.; Bonacic-Koutecky, V. *J. Chem. Phys.* **2001**, *114*, 2106−2122.

(18) Michl, J.; Bonačić-Koutecký, V. *Electronic Aspects of Organic Photochemistry*; Wiley: New York, 1990.

(19) Bernardi, F.; Olivucci, M.; Robb, M. A. *Chem. Soc. Rev.* **1996**, *25*, 321−329.

(20) Domcke, W.; Stock, G. *Adv. Chem. Phys.* **1997**, *100*, 1−169.

(21) Reischl, B.; de Vivie-Riedle, R.; Rutz, S.; Schreiber, E. *J. Chem. Phys.* **1996**, *104*, 8857−8864.

(22) Erdmann, M.; Engel, V. *J. Chem. Phys.* **2004**, *120*, 158−164.

(23) Tully, J. C. *Faraday Discuss.* **1998**, *110*, 407−421.

(24) Berne, B. J.; Ciccotti, G.; Coker, D. F. *Quantum and Classical Dynamics in Condensed Phase Simulations*; World Scientific: Singapore, 1998.

(25) Gindensperger, E.; Meier, C.; Beswick, J. A. *Adv. Quantum Chem.* **2004**, *47*, 331−346.

(26) Stock, G.; Thoss, M. *Adv. Chem. Phys.* **2005**, *134*, 243−375.

(27) Stock, G.; Miller, W. H. *Chem. Phys. Lett.* **1992**, *197*, 396−404.

(28) Yu, N.; Margulis, C. J.; Coker, D. F. *J. Chem. Phys.* **2004**, *120*, 3657−3664.

(29) Hartmann, M.; Pittner, J.; Bonačić-Koutecký, V. *J. Chem. Phys.* **2001**, *114*, 2123-2136.

(30) Lax, M. *J. Chem. Phys.* **1952**, *20*, 1752−1760.

(31) Stock, G.; Thoss, M. *Phys. Rev. Lett.* **1997**, *78*, 578−581.

(32) Meyer, H.-D.; Miller, W. H. *J. Chem. Phys.* **1979**, *70*, 3214−3223.

(33) Stock, G.; Miller, W. H. *J. Chem. Phys.* **1993**, *99*, 1545−1555.

(34) Dilthey, S.; Mehlig, B.; Stock, G. *J. Chem. Phys.* **2002**, *116*, 69−78.

(35) Wang, H.; Thoss, M. *J. Phys. Chem. A* **2003**, *107*, 2126−2136.

(36) Jortner, J.; Bixon, M. *Electron Transfer*: *From Isolated Molecules to Biomolecules*; Wiley: New York, 1999; Adv. Chem. Phys. Vols. 106−107.

(37) Köppel, H.; Domcke, W.; Cederbaum, L. S. *Adv. Chem. Phys.* **1984**, *57*, 59−246.

(38) Marcus, R. A.; Sutin, N. *Biochim. Biophys. Acta* **1985**, *811*, 265−322.

(39) Yan, Y. J.; Mukamel, S. *Phys. Rev. A: At., Mol., Opt. Phys.* **1990**, *41*, 6485−6504.

(40) Pollard, W.; Lee, S.-Y.; Mathies, R. A. *J. Chem. Phys.* **1990**, *92*, 4012−4029.

(41) Thoss, M.; Stock, G. *Phys. Rev. A: At., Mol., Opt. Phys.* **1999**, *59*, 64−79.

(42) The mapping of the operators in eq 3.4 preserves the commutation relations and leads to an exact identity of the electronic matrix elements of the propagator.[31]

(43) Müller, U.; Stock, G. *J. Chem. Phys.* **1998**, *108*, 7516−7526.

(44) Rabani, E.; Egorov, S. A.; Berne, B. J. *J. Phys. Chem. A* **1999**, *103*, 9539−9544.

(45) Dilthey, S.; Stock, G. *Phys. Rev. Lett.* **2001**, *87*, 140404.

(46) Liao, J.-L.; Voth, G. A. *J. Phys. Chem. B* **2002**, *106*, 8449−8455.

(47) Shalashilin, D. V.; Child, M. S. *J. Chem. Phys.* **2004**, *121*, 3563−3568.

(48) Novikov, A.; Kleinekathöfer, U.; Schreiber, M. *Chem. Phys.* **2004**, *296*, 149−158.

(49) Shi, Q.; Geva, E. *J. Phys. Chem. A* **2004**, *108*, 6109−6116.

(50) Grossmann, F. *Phys. Rev. A: At., Mol., Opt. Phys.* **1999**, *60*, 1791−1796.

(51) Thoss, M.; Miller, W. H.; Stock, G. *J. Chem. Phys.* **2000**, *112*, 10282−10292.

(52) Bonella, S.; Coker, D. *Chem. Phys.* **2001**, *268*, 189−200.

(53) Bonella, S.; Coker, D. F. *J. Chem. Phys.* **2005**, *122*, 194102.

(54) Stock, G. *J. Chem. Phys.* **1995**, *103*, 2888−2902.

(55) Dietz, H.; Engel, V. *J. Phys. Chem. A* **1998**, *102*, 7406−7413.

(56) Dilthey, S.; Hahn, S.; Stock, G. *J. Chem. Phys.* **2000**, *112*, 4910−4922.

(57) Seidner, L.; Stock, G.; Domcke, W. *J. Chem. Phys.* **1995**, *103*, 3998−4011.

(58) Dilthey, S.; Stock, G. *J. Phys. Chem. A* **2002**, *106*, 8483−8487.

(59) Stock, G.; Domcke, W. *Phys. Rev. A: At., Mol., Opt. Phys.* **1992**, *45*, 3032−3040.

(60) Kambhampati, P.; Song, D. H.; Kee, T. W.; Barbara, P. F. *J. Phys. Chem. A* **2000**, *104*, 10637−10644.

CT6002127